Experimental Lab: Examination of the Wake behind Aerodynamic Bodies

Grant Norman
Univeristy of Colorado at Boulder

I. Introduction

This lab aims to investigate the changes in the flow field caused by a circular cylinder and by a Clark Y-14 airfoil, at airspeeds of 15 m/s and 25 m/s. First, the wake is analyzed as a function of the flow speed, the body's shape, and the body's location. Second, the quantitative changes to the flow field are used to calculate the coefficient of drag of the aerodynamic body.

The flow field is characterized by the speed field, $u(x, y)$, which tells the speed at a location (x, y), in $\frac{meters}{second} = m/s$. The x coordinate is the distance measured from the trailing edge of the body, towards the back of the wind tunnel, while the y coordinate is the distance above the trailing edge, both in $millimeters = mm$. The freestream airspeed is denoted by u_∞, which also corresponds to the *upstream* airspeed. The entire flow is assumed to be horizontal, meaning that the flow of interest is always parallel to the sides of the wind tunnel test section. Thus, the velocity deficit is defined as $\Delta u(x, y) = u_\infty - u(x, y)$, representing the loss in horizontal velocity. Similarly, $\delta(x)$ is half of the width of the wake in mm, corresponding to the average distance perpendicular from the x axis, back to a location where the speed is approximately the free stream speed.

The control volume is defined as the region of space where the drag of the body is the only noticeable body force. This region extends horizontally from a sufficiently upstream location (where u_∞ is constant) to the selected downstream location. Vertically, the region starts and ends at the edge of the boundary layers created by the walls of the test section. However, this control volume *excludes* the body.

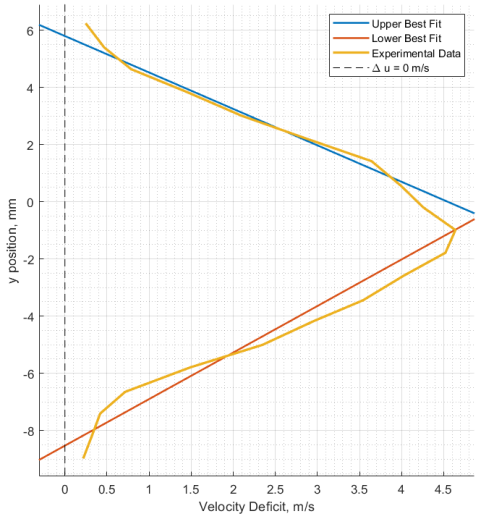

Fig. 1 Example Velocity Deficit with Linear Best Fits

From wind tunnel data of dynamic pressure $(p_0 - p)$ and density (ρ), the speed is calculated by rearranging Bernoulli's Equation into Eq. 1.

$$u(x, y) = \sqrt{\frac{2 \cdot (p_0 - p)}{\rho}} \tag{1}$$

II. Methodology

A. Experimental Setup

The data used is a combination of many individual data sets. Each data set is a collection of 20 different heights at a constant horizontal position. The upstream data was usually measured at evenly spaced heights, while the downstream data was focused on the wake profile. Various techniques were employed in deciding where to measure along the wake, although a better wake profile is constructed by placing more measurement points where the speed changes quickly. Thus, the wake location was identified, a few baseline points were taken above and below the wake leaving most measurement locations placed within the wake. The distribution of measurements within the wake was roughly

linear, with slight adjustments to better capture regions where the speed changed quickly. The same vertical locations were also sampled upstream.

B. Upstream Simplification

In the analysis of the flow, it is assumed that the relevant upstream velocity profile is of constant magnitude. All of the upstream data were combined to yield the speed profiles shown in Fig. 2. There is no correlation with height and speed, other than the fact that there are more samples closer to $y = 0$ mm. The mean airspeeds were 14.8 ± 0.4 m/s and 24.9 ± 0.3 m/s, with 92% of the data falling within each of their respective ranges. Thus, *it is reasonable to assume that the upstream airspeed is constant at the mean values and is independent of vertical position.*

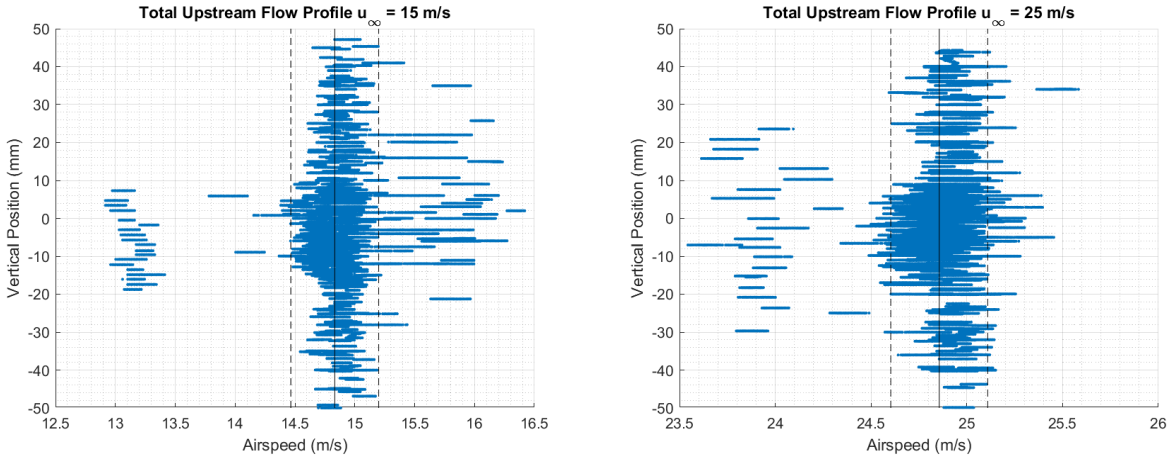

Fig. 2 Total Upstream Flow Profile for $u_\infty = 15$ m/s (Left) and $u_\infty = 25$ m/s (Right)

C. Velocity Deficit Profile

Each testing location will reveal the profile of the aforementioned velocity deficit. Figure 1 shows an example deficit along with best-fit lines. These lines are used to extrapolate an estimate of the width of the wake by predicting when $\Delta u(x, y)$ is sufficiently close to 0 m/s. Each profile yields two predictions for $\delta(x)$, which are then averaged to give the final value of $\delta(x)$ for that horizontal location.

Further, the velocity deficit profiles and the wake half-widths may be non-dimensionalized as the variables $\mu(x, y)$ and $\Upsilon(x)$, respectively, as shown in Eq. 2 and 3.

$$\mu(x, y) = \frac{\Delta u(x, y)}{\Delta u_{max}(x)} \tag{2}$$

$$\Upsilon(x) = \frac{y}{\delta(x)} \tag{3}$$

III. Results

A. Dimensional Wake Profiles

As mentioned above, the wake profile is shown by considering the velocity deficit, $\Delta u(x, y)$. This profile changes as a function of horizontal position, the upstream body, and the airspeed. Figures 3-6 show the development of the wake for each configuration. For both geometries, a higher airspeed results in a deeper wake — $\Delta u(x, y)$ is greater. Also, *the wake of the cylinder is much larger than the wake of airfoil*, so different scales are used to clarify other points of comparison.

Generally, the airfoil produces a more chaotic wake than the cylinder, which is shown in the majority of the data presented in this report. Specifically, Fig. 5 shows that velocity profiles at the same x location can be very different (consider the profiles starting at $x = 17$ mm). In the analysis of this data, these profiles are combined through utilization of best fit curves, meeting the recommendation outlined in the Lab Document (Source [1]).

In all cases (Fig. 3-6), the wake's influence (width) increases as it travels downstream, in exchange for the maximum deficit decreasing. This is best described as *momentum diffusing between fluid elements*, which corresponds to the $-\mu\nabla^2$ term in the Navier-Stokes Momentum Equations. This is shown in Eq. 4 with gravity as the only body force for the region of interest, which is after the body has already been encountered.

$$\rho\frac{D\mathbf{V}}{Dt} = -p\nabla + \rho\mathbf{g} - \mu\nabla^2 \tag{4}$$

The wake in the airfoil cases (Fig. 5 and 6) is located below airfoil, more prominently in the $u_\infty = 15$ m/s case. This is likely due to the asymmetry of the airfoil's pressure distribution, as opposed to the symmetric pressure distribution of the cylinder. Because the wake is located below the horizontal, the air coming from the upper half of the airfoil must have had higher speed than the air from the bottom half of the airfoil. In Fig. 6 inertial effects are more prominent (higher Reynolds number *Re*), but the wake is closer to the horizontal. This suggests that the vertical location of the center of the wake is influenced most by viscous effects. While the influence of the body force term ρg in Eq. 4 can also explain the wake being centered below the horizontal, this is not seen in the cylinder cases, which are equally influenced by gravity as the airfoil cases.

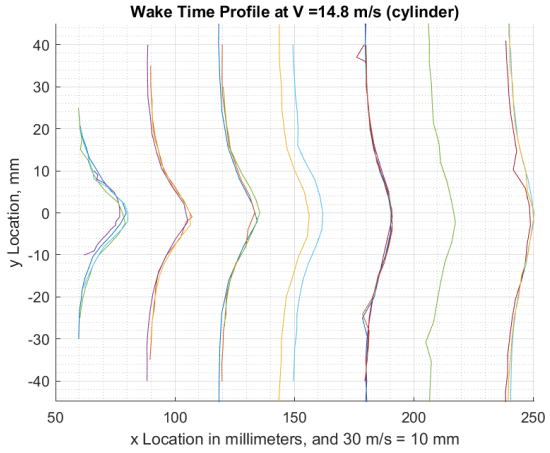

Fig. 3 Wake Development for Cylinder at 15 m/s

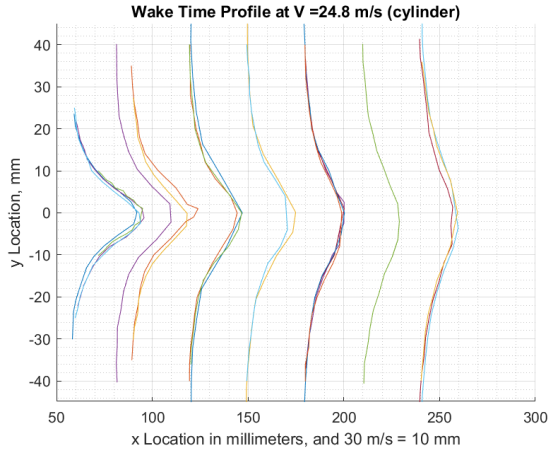

Fig. 4 Wake Development for Cylinder at 25 m/s

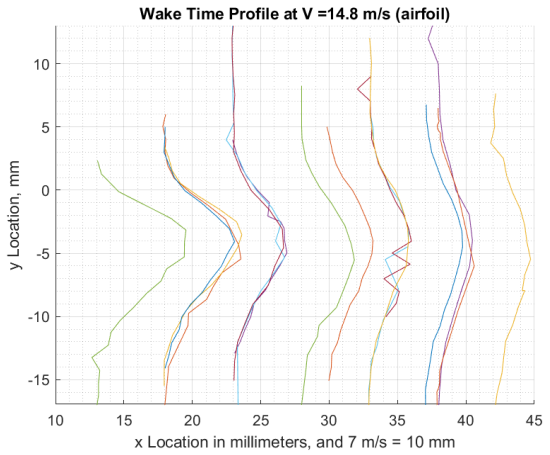

Fig. 5 Wake Development for Airfoil at 15 m/s

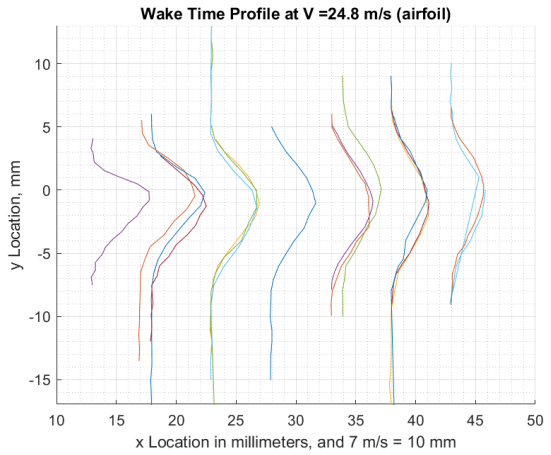

Fig. 6 Wake Development for Airfoil at 25 m/s

B. Quantitative Wake Growth

By using the linear approximation method outlined in Section II.C, the half width of the wake $\delta(x)$ can be calculated for each data set. The growth of the wake is quantitatively shown in Fig. 7. For the cylinder, the wake seems to grow at approximately a linear rate, as shown by the best-fit lines. The airfoil wake's growth is less predictable, weakly suggesting that the airfoil wake grows at less than a linear rate (potential modeled by a square-root function).

Similarly, Fig. 8 shows that the maximum velocity deficit decreases with increasing horizontal distance. Thus, momentum is being diffused from a centralized high velocity deficit, to a more dispersed, lower deficit. Again, this corresponds to the $-\mu\nabla^2$ viscosity term in Eq. 4, which emulates the equation for the diffusion of heat through a medium. This diffusion should also be considered as occurring between moving fluid elements, as the velocity deficit, rather than the velocity itself is being considered. **In sum, the momentum change caused by the presence of a body increasingly diffuses through the medium, losing strength in exchange for a greater area.** This process occurs at a faster rate for the airfoil than the cylinder, as the airfoil has more extreme slopes in Fig. 7 and 8. This difference may exist due to the airfoil producing a more chaotic initial wake, which influences a greater region of space than the cylinder's consistent wake. Mathematically, the cylinder is closer to its steady-state solution.

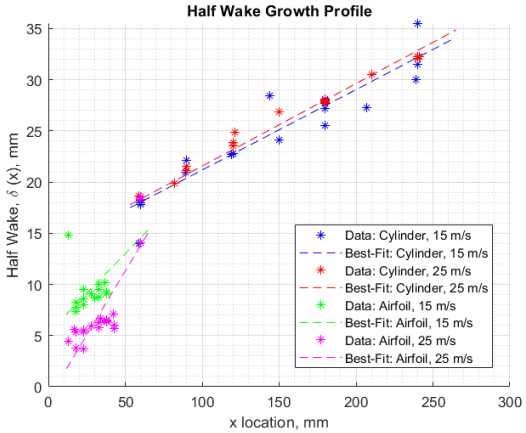

Fig. 7 Half Width Wake Growth, $\delta(\mathbf{x})$

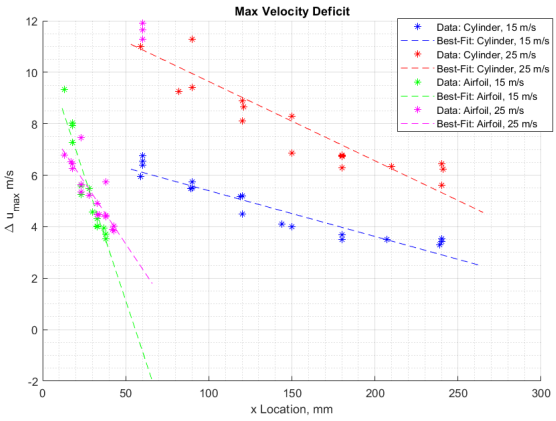

Fig. 8 Max Velocity Deficit Change, $\Delta\mathbf{u_{max}}(\mathbf{x})$

C. Non-Dimensional Wake Growth

By using Eq. 2 and 3, the velocity deficits and vertical positions were non-dimensionalized as $\mu(x, y)$ and $\Upsilon(x)$. Note that μ is also used to denote the kinematic viscosity coefficient, but the context of usage will clearly indicate which μ is being referenced. Figures 9 and 10 show the non-dimensionalized wake profiles. Note that the same trends observed in Section III.A are still apparent. The airfoil profiles are centered below the horizontal, with the 15m/s profile being farther from the horizontal. For the two cylinder cases, the wake is self-similar. Figure 10 shows the 15m/s case in blue and the 25m/s case in red. Other than the start (small x values), these curves map directly onto each other so precisely that it is hard to distinguish two separate curves. However, the airfoil cases do not exhibit self-similarity, as the Clark-Y airfoil is asymmetric.

D. Drag Coefficients

Using the control volume defined in Section I, drag is added to the integral form of Eq. 4. Then by assuming that there are no viscous or other body forces in the steady flow, drag is rewritten as Eq. 5 from Source [2], by also using the Continuity Equation. Physically, this means that the magnitude of the change in momentum of the flow is equivalent to drag of the body. Equation 5 is then non-dimensionalized by dividing by $\frac{1}{2}\rho u_\infty^2 \cdot c$, where c is the reference length (chord) of the body. Computationally, the coefficients of drag for each individual profile may be found through a trapezoidal approximation of Eq. 6.

$$D' = \int_{y_{min}}^{y_{max}} \rho \cdot u_\infty \cdot \Delta u(x_i, y) dy \tag{5}$$

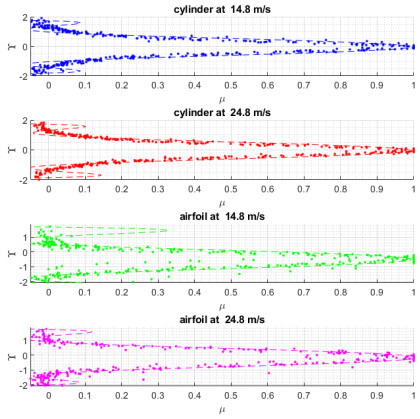

Fig. 9 Non-dimensionalized Wake Profiles, Separate

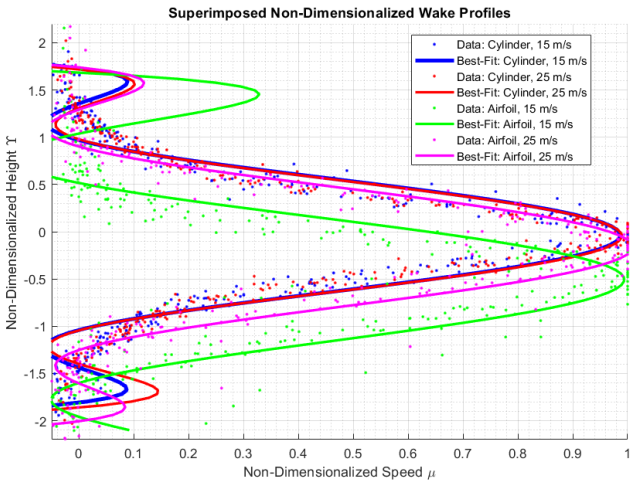

Fig. 10 Non-dimensionalized Wake Profiles, Combined

$$C_d = \frac{2}{u_\infty c} \cdot \int_{y_{min}}^{y_{max}} \Delta u(x_i, y) dy \tag{6}$$

For the cylinder at 15m/s and 25m/s, the coefficients of drag were found as $\mathbf{1.1 \pm 0.1}$ and $\mathbf{1.2 \pm 0.1}$, respectively. The corresponding drag coefficients for the airfoil were calculated as $\mathbf{0.08 \pm 0.1}$ and $\mathbf{0.03 \pm 0.1}$. These enormous error bounds reflect the variance of repeated experiments, as discussed in Section III.A. The means were calculated by excluding outliers greater than three times the mean.

E. Existing Experimental Data

The temperature is used to approximate the dynamic viscosity, μ. Combining this with physical and wind tunnel data, the Reynolds numbers are found, yielding values of $1.06 \cdot 10^4$, $1.77 \cdot 10^4$, $7.39 \cdot 10^4$, and $1.24 \cdot 10^5$ for the cylinder at 15m/s and 25m/s and for the airfoil at 15m/s and 25m/s, respectively.

Source [2] provides experimentally measured drag coefficients for various Reynold's numbers, with $V_\infty = 15$ m/s and $V_\infty = 25$ m/s both corresponding to roughly $C_d = 1.2$. Thus, the experimental values of 1.1 ± 0.1 and 1.2 ± 0.1 are reasonable.

Source [3] similarly gives estimates of coefficients of drag for the Clark-Y airfoil at various Reynolds numbers. At $Re = 50000$, $C_d = 0.03$, and at $Re = 100000$, $C_d = 0.02$. Thus, the experimentally calculated coefficients of drag are farther from other calculated values, yet in the same direction. This indicates that the experimental error was likely a systematic error. The derivation of Eq. 5 assumes that there are no viscous forces within the fluid. However, Fig. 7 and 8 imply that momentum is diffused, which occurs *through viscous effects*. Thus, in the experiments, the calculated drag coefficient is an overestimate, as it also includes the viscous effects of the fluid as momentum diffuses. Closer to the aerodynamic body, the drag coefficient would be calculated as closer to the referenced values, as less viscous effects within the fluid have occurred.

IV. Conclusions

This lab examined the wake formed behind a cylinder and an airfoil while implementing a control volume system for determining sectional drag coefficients. It was observed that the momentum deficit diffused through the fluid in a manner analogous to heat diffusion. From this analogy, as the horizontal distance approaches infinity, the wake is predicted have an infinitely small deficit, spread across an infinite vertical wake. The airfoil seemed to approach this steady-state solution at a quicker rate than the cylinder, as shown by its quicker wake growth, and its quicker velocity deficit change (Fig. 7 and 8). This diffusion is described by the $-\mu\nabla^2\mathbf{V}$ term in the Navier-Stokes equations, again mirroring the form of the heat equation. The Navier-Stokes equations were also combined with the continuity equation and applied to a simple control volume to determine an expression for the drag coefficient in this scenario. It was assumed that viscous effects within the fluid were minimal, contrary to the preceding discussion of viscosity as the means of momentum diffusion. Nonetheless, the drag coefficients of the cylinder and airfoil were calculated from each setup, with reasonable cylinder coefficients of drag, and overestimates for the coefficients of drag of the airfoil.

V. Acknowledgements

Specific Acknowledgements are included in the MATLAB code.

References

[1] "Aerodynamics Experimental: Examination of the Wake behind Aerodynamic Bodies," https://canvas.colorado.edu/courses/54083/files/7126300?module_item_id=1527119, 2019. Online; accessed 24 October 2019.

[2] Anderson, J., *Fundamentals of Aerodynamics*, McGraw-Hill Education, 2 Penn Plaza, New York, NY 10121, 2017.

[3] "Airfoil Tools: Clark Y Airfoil," http://airfoiltools.com/airfoil/details?airfoil=clarky-il, 2019. Online; accessed 24 October 2019.